DEPARTAMENT D'ASTRONOMIA I METEOROLOGIA

Near-relativistic electron events. Monte Carlo simulations of solar injection and interplanetary transport

Memòria presentada per
Neus Àgueda Costafreda
per optar al grau de Doctora
per la Universitat de Barcelona.
Barcelona, 20 de febrer de 2008

3 Interplanetary particle transport model

Solar energetic particles can travel through the heliosphere with a negligible chance of hitting each other or even of hitting one of the much more numerous particles of thermal energy which constitute the solar wind. Their trajectories are shaped by the interplanetary magnetic field (IMF) that can be characterized by a smooth average field, represented by an Archimedean spiral (Parker 1958) with superimposed irregularities.

Unfortunately, there is no way to observe the complete trajectory of an individual energetic particle from its source to the spacecraft position. What is measurable is the intensity of charged particles as a function of time, energy and direction of incidence (normally related to the local direction of the magnetic field) in a given point of the heliosphere where the spacecraft is located. Our aim is to understand the propagation of solar energetic particles along the IMF. Only when the interplanetary transport conditions are well understood, it is possible to draw conclusions about the solar source from the analysis of particle observations.

In the first section of this chapter, we briefly review the processes relevant to the transport of energetic particles along the IMF, as well as the characteristics of the main numerical methods that have been used to solve the transport equation. The following three sections are devoted to the description of the Monte Carlo model of particle transport, developed to study the transport of solar near-relativistic electrons. The last section describes the tests performed to ensure that the model works properly.

3.1 Interplanetary particle transport models

An assumption that can be reasonably made is that the motion of energetic particles along the IMF consists of two components: adiabatic motion along the smooth field and pitch-angle scattering caused by superimposed irregularities (Roelof 1969). The transport of energetic particles perpendicular to the average magnetic field can be neglected in the inner heliosphere (radial distances from the Sun smaller than ten solar radii) because particles move much

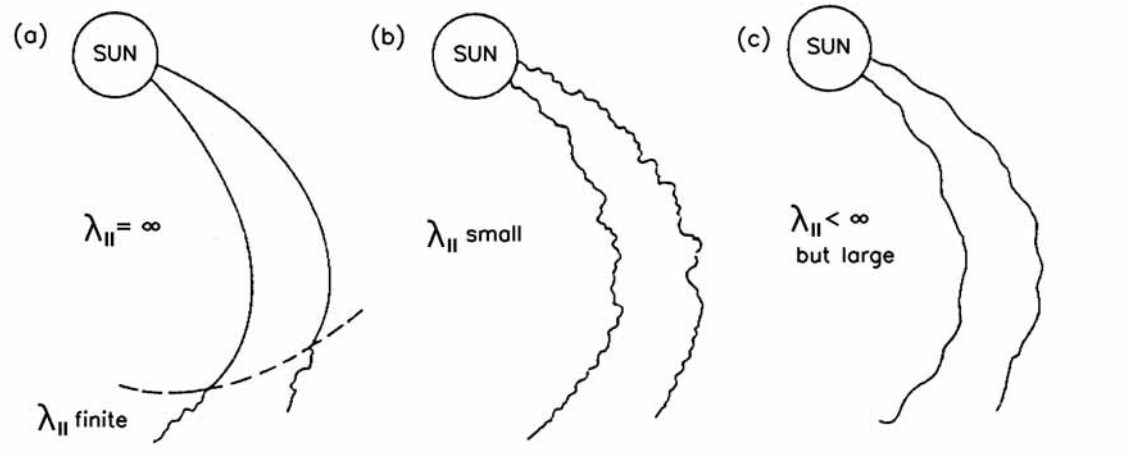

Figure 3.1: Propagation schemes for various degrees of turbulence superimposed on the average Archimedean field: (a) scatter-free transport (with a boundary), (b) diffusive transport, and (c) focused transport (adapted from Kunow et al. 1991). The mean free path along the field line, $\lambda_{\|}$, is related to the degree of turbulence in the IMF.

smaller distances per time unit in the perpendicular direction than in the parallel direction (e.g. Bieber et al. 1995; Zank et al. 1998).

The nature of particle propagation varies considerably with the relative strength of the two processes influencing the motion of energetic particles along the IMF. Two idealized models describe most extreme situations, that is, scatter-free transport and diffusive transport. Particle transport is scatter-free if particle propagation occurs in a sufficiently smooth magnetic field where the superimposed irregularities play a weak role. Particle transport is diffusive if the pitch-angle scattering is strong; then, particle propagation is described by spatial diffusion with a small mean free path. In an intermediate case, the transport is focused and both pitch-angle scattering and adiabatic motion along the average IMF are relevant. Figure 3.1 sketches these three propagation scenarios.

3.1.1 Scatter-free transport

Scatter-free transport conditions assume that the particle motion is exclusively determined by the averaged IMF; therefore, pitch-angle scattering by field fluctuations is neglected. In the particular case depicted in Figure 3.1(a) the scatter-free regime extends up to a certain distance from the Sun, beyond which there is an increase of the scattering processes. Nolte & Roelof (1975) presented the mathematical formulation to describe the scatter-free propagation of energetic particles for this particular case.

Particle motion along a prescribed magnetic field is normally separated into two parts: the motion of the guiding center of the particle orbit and the gyration of the particle around it.

The motion of the guiding center can be interpreted as the effective motion of the particle, averaged over many gyrations. The particle pitch-angle cosine, μ, is defined as the cosine of the angle between the particle velocity and the magnetic field vector; it is given by

$$\mu = \cos\alpha = \frac{v_{\parallel}}{v} \tag{3.1}$$

where α is the pitch-angle, v is the particle velocity and $v_{\parallel}$ is the velocity component parallel to the magnetic field. If v is constant along the motion, μ reflects the proportion of particle kinetic energy that corresponds to translation along the IMF line.

In collisionless plasmas, the magnetic moment, also called the first adiabatic invariant, $\Gamma = p_{\perp}^2/2B$, remains constant in a slowly varying magnetic field[1]. Thus, if the particle speed remains constant, the quantity $\sin^2\alpha/B$ is also constant. This means that the particle pitch-angle decreases when the particle moves toward a region where the magnetic field strength decreases, i.e. the particle motion becomes more focused in the field direction. For a Parker spiral magnetic field in the ecliptic plane, the strength varies as

$$B(r) = B_0 \left(\frac{r_0}{r}\right)^2 \sec\psi(r) \tag{3.2}$$

where r_0 is the radial distance from the center of the Sun at which the field is frozen into the solar wind, $B_0 = B(r_0)$, and ψ is the angle between the radial direction and the local magnetic field, given by

$$\sec\psi(r) = \sqrt{1 + \left(\frac{\Omega}{u}\right)^2 r^2} \tag{3.3}$$

where Ω is the sidereal solar rotation rate and u is the solar wind speed. It is worth noting that since the magnetic flux, $\Phi = B \cdot \sigma$, is constant, the cross-sectional area of the magnetic flux tube, σ, scales as $\sigma \propto B^{-1} \propto r^2 \ \sec^{-1}\psi(r) = r^2 \ \cos\psi(r)$.

For charged particles moving away from the Sun, as B decreases with the radial distance, α also decreases. This is called the focusing effect because it yields to a collimation of the particles to the field lines. Particles injected isotropically at 2 $R_\odot$ appear to come in a narrow cone only $\sim 1^\circ$ wide to an observer located at 1 AU (assuming $u = 400$ km s^{-1}). On the other hand, for particles moving toward the Sun, as B increases, α also increases. When $\alpha = 90^\circ$ ($\mu = 0$), particles reach the mirror point, where they only gyrate. After that, they again propagate towards the decreasing B.

[1] The field changes slowly when the characteristic scale of the magnetic field variations is large compared to the gyroradius of the particle.

Given a mono-energetic impulsive injection of particles from the Sun and under the scatter-free transport approximation, the peak intensities and fluences of a solar energetic particle event observed at different radial positions scale like $\propto \sigma^{-1}$.

3.1.2 Focused transport

If particles undergo pitch-angle scattering processes due to some degree of turbulence in the IMF, they arrive at the observer in a wider cone of pitch-angles than they would do in a scatter-free medium. In the focused transport approximation, the evolution of the distribution function, $f(z, p, \mu, t)$, which gives the number of particles per unit volume of the six-dimensional phase space $(\vec{r}, \vec{p})$, is governed by the particle streaming along the magnetic field lines, the scattering processes off the fluctuations of the magnetic field and the magnetic focusing (i.e., mirroring) in the outward decreasing magnetic field. The distribution function is a function of the coordinate measured along the mean magnetic field, z, the particle momentum, p, the cosine of pitch-angle, μ, and time t.

The equation governing the evolution of the particle distribution function is the focused transport equation (Roelof 1969) given by

$$\frac{\partial f}{\partial t} + v\mu\frac{\partial f}{\partial z} + \frac{1-\mu^2}{2L}v\frac{\partial f}{\partial \mu} = \frac{\partial}{\partial \mu}D_{\mu\mu}\frac{\partial f}{\partial \mu} \tag{3.4}$$

where the second term on the left hand side describes streaming of particles along the magnetic field lines, the third term on the left hand side describes the focusing of particles and the term on the right hand side accounts for the effect of magnetic fluctuations, which is modeled by pitch-angle diffusion. The particle speed, v, remains constant in this model, in which the magnetic field is assumed to be static. The IMF systematic effect is characterized by the focusing length, L, given by

$$\frac{1}{L(z)} = -\frac{1}{B(z)}\frac{\partial B}{\partial z}, \tag{3.5}$$

and the stochastic forces are described by a pitch-angle diffusion coefficient, $D_{\mu\mu}$. Equation (3.4) still neglects adiabatic deceleration and solar wind convection effects. Ruffolo (1995) deduced the explicit transport equation for the focused transport of energetic particles, including adiabatic deceleration and solar wind convection effects.

The quasilinear theory (QLT) assumes that the irregularities superposed on the average magnetic field are sufficiently small such that the interaction between waves and particles is

considered to the first order only; higher order terms in the disturbances are small enough to be neglected. Based on this assumption, it is possible to derive the pitch-angle diffusion coefficient (Jokipii 1966; Hasselmann & Wibberenz 1968). "Small irregularities" means that changes in pitch-angle during a single gyration are small and several gyrations are required to considerably modify the particle pitch-angle. This implies that particles are scattered by magnetic irregularities which are in resonance with the particle gyration. As a cumulative result of many small random changes in pitch-angle, charged particles experience a macroscopic change in direction. A particular case happens when these fluctuations are transverse and axially symmetric, with wave vectors parallel to the average field. Then, particles with gyration time T_g experience resonant influences from irregularities with wavenumbers k when they travel a distance $v_\parallel T_g = 2\pi/k$ along the field (see Figure 3.2a). This case is referred as the "slab model". The combination of the QLT with the slab model is known as the "standard model" of particle scattering (Jokipii 1966; Jaekel & Schlickeiser 1992).

Jokipii (1966) explicitly derived the pitch-angle diffusion coefficient in terms of the power spectrum of the fluctuating field. If the power spectrum of the fluctuating field can be represented by a power law,

$$P(k) \propto k^{-q} \tag{3.6}$$

where k is the wavenumber parallel to the magnetic field and q is the spectral slope of the magnetic field power spectrum, then the standard model predicts a pitch-angle diffusion coefficient of the form

$$D_{\mu\mu} = \frac{\nu}{2}(1-\mu^2) \tag{3.7}$$

where ν is the scattering frequency, proportional to the power spectrum of the magnetic fluctuations in the neighborhood of the resonant wave number $k = 2\pi/v_\parallel T_g$. The scattering frequency takes the form

$$\nu(\mu) = \nu_0 |\mu|^{q-1} \tag{3.8}$$

with $\nu_0 = 6v/[2\lambda_\parallel(4-q)(2-q)]$.

Measured magnetic field spectra give spectral slopes in the range $1.3 \leq q \leq 1.9$ with an average value of $q = 1.63$ (Kunow et al. 1991). Figure 3.2(b) shows the shape of the pitch-angle diffusion coefficient for different slopes of the magnetic field power spectrum and $\lambda_\parallel = 0.5$ AU. The scattering is isotropic when $q = 1$, i.e. when the strength of the scattering is independent of the pitch-angle of the particles, $\nu = \nu_0$; then the diffusion coefficient is given

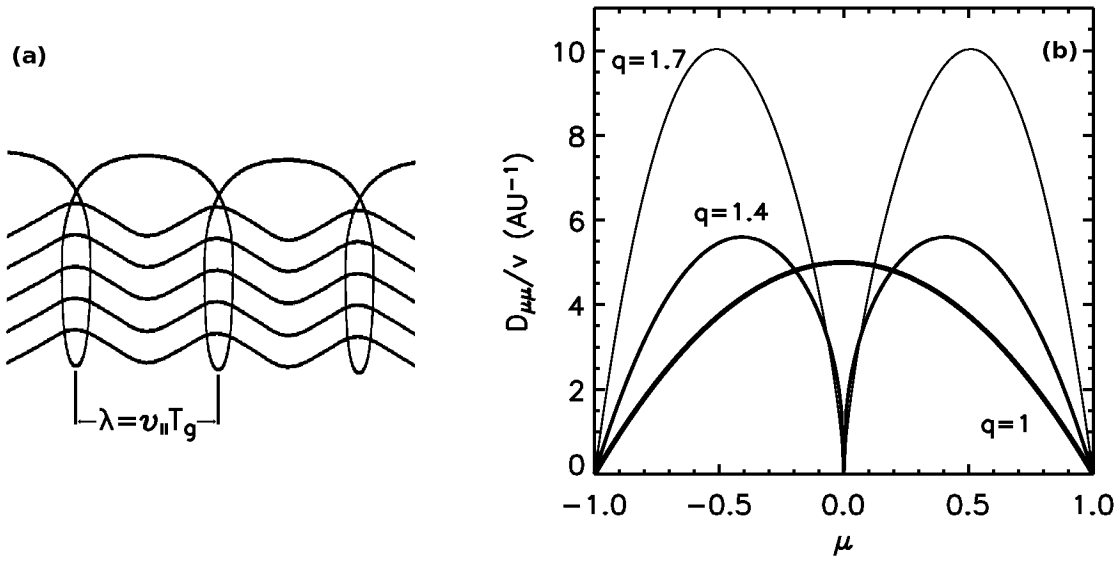

Figure 3.2: (a) Resonance scattering: the particle interacts with waves (λ is the wavelength) in resonance with its motion parallel to the magnetic field (from Kallenrode 2004). (b) Shape of the standard pitch-angle scattering coefficient for different slopes q of the power spectrum of the fluctuating magnetic field.

by $D_{\mu\mu} = \nu_0(1-\mu^2)/2$. As the power spectrum becomes steeper, particles with pitch-angles close to 90° experience less scattering[2] and therefore, a gap develops around $\mu = 0$ with increasing slope of the magnetic field spectrum. For $q \geq 2$ the gap around $\mu = 0$ becomes too wide to scatter particles through 90°. Thus, the particle transport is totally decoupled in two hemispheres (parallel and anti-parallel to the magnetic field vector).

The relation between $D_{\mu\mu}$ and the parallel scattering mean free path $\lambda_\parallel$ is given by (Hasselmann & Wibberenz 1968, 1970)

$$\lambda_\parallel = \frac{3v}{8}\int_{-1}^{1}\frac{(1-\mu^2)^2}{D_{\mu\mu}}d\mu = \frac{3v}{4}\int_{-1}^{1}\frac{1-\mu^2}{\nu(\mu)}d\mu \tag{3.9}$$

This definition is valid under two basic assumptions: slow time dependence (near stationarity) and strong scattering. Therefore, at the limit of weak scattering, the physical meaning of the $\lambda_\parallel$ parameter is questionable. A relevant discussion on this point can be found in Qin et al. (2005).

[2]Particles with large pitch-angles are in resonance with waves with small wavelengths. Since the power density spectrum decreases toward high wave numbers, there is not enough power left for efficient scattering (Kallenrode 2004).

3.1.3 Diffusive transport

In the context of a highly turbulent medium, pitch-angle scattering by field fluctuations can change the pitch-angle of the particles by more than 90° and cause a stochastic motion back and forth along the average field. Under this approach, particle transport is considered to be simply diffusion, and solar wind expansion effects are neglected. Then, Equation (3.4) reduces to

$$\frac{\partial n}{\partial t} = \frac{1}{\sigma}\frac{\partial}{\partial z}\left(\sigma D_{\parallel}\frac{\partial n}{\partial z}\right) \tag{3.10}$$

for the particle density per unit momentum $n(r,t) = d^4N/(d^3r\,dp)$. In this approximation the spatial diffusion coefficient, $D_{\parallel}$, is related to the parallel mean free path, $\lambda_{\parallel}$, by

$$D_{\parallel} = \frac{1}{3}v\lambda_{\parallel}. \tag{3.11}$$

Hence, the mean free path of the particles parallel to the magnetic field can be directly related to the amount of fluctuations in the IMF.

Equation (3.10) can be expressed in terms of a radial diffusion equation by a transformation of the spatial coordinate measured along the field line, z, to the radial distance, r, by

$$\frac{\partial n}{\partial t} = \frac{1}{r^2}\frac{\partial}{\partial r}\left(r^2 D_{rr}\frac{\partial n}{\partial r}\right) \tag{3.12}$$

where $D_{rr} = D_{\parallel}\cos^2\psi$ is the radial diffusion coefficient and ψ is the angle between the field line and the radial direction. Equation (3.12) has the attractive feature that it can be analytically solved for an impulsive injection of particles from the Sun and under the assumption that $D_{rr} \propto r^b$ with $b < 2$ (Wibberenz et al. 1989). The solution is given by

$$n(r,t) = \frac{dN}{dp}\frac{1}{r^3}\frac{2-b}{\Gamma(3/(2-b))}\left(\frac{r^2}{(2-b)^2 D_{rr}t}\right)^{3/(2-b)}\exp\left(-\frac{r^2}{(2-b)^2 D_{rr}t}\right) \tag{3.13}$$

where dN/dp is the momentum spectrum of particles injected in the interplanetary medium per steradian at the solar surface. If the injection is extended in time, the solution of the transport equation can be obtained by using Equation (3.13) as a Green's function, i.e. convolving the function with an extended injection profile $Q(E,t)$.

The assumption of diffusive transport is so strong that it can only be applied to the study of a limited fraction of SEP events. It does, however, have relevant applications in the study of the transport of galactic and anomalous cosmic rays in the heliosphere. For more general

considerations, such as for modeling the spatial dependence of SEP event peak fluxes or event fluences, the diffusive assumption gives a reasonable starting point.

Vainio et al. (2007) derived the spatial scaling laws of peak intensities, fluences and time-integrated net fuxes obtained from the analytical solution of the diffusion equation[3]. These are: (1) the time of maximum intensity scales like $\propto r^{-3}$; (2) the time-integrated intensity (or fluence) scales like $\propto (rD_{rr})^{-1}$; and (3) the time-integrated radial net flux scales like $\propto r^{-2}$.

3.1.4 Numerical methods: finite-differences and Monte Carlo

Several authors (e.g. Ma Sung & Earl 1978; Ng & Wong 1979; Heras et al. 1992; Ruffolo 1995; Torsti et al. 1996; Kocharov et al. 1998; Lario et al. 1998; Vainio 1998; Hatzky & Kallenrode 1999; Dröge 2000; Li et al. 2003; Maia et al. 2007; Agueda et al. 2008) have developed transport models to simulate the interplanetary transport of energetic particles injected at the root of a spiral IMF line.

The focused transport equation, including adiabatic deceleration and solar wind convection effects[4], was first solved by Ruffolo (1995) by means of a finite-difference numerical method. The transport equation was solved using a mixed coordinate system, where particle velocity is measured in the solar wind frame and spatial coordinate and time are measured in the frame corotating with the Sun. Ruffolo (1995) applied operator splitting, that is, the particle distribution function was updated according to each term of the equation every time step. This can be interpreted as particles sequentially streaming along the field, and undergoing pitch-angle scattering and focusing during each time step. As the time step was shortened, this sequence provided a more accurate approximation to the simultaneous action of these processes. Lario et al. (1998) developed a particle transport model also based in the finite-difference numerical method. This latter model included a mobile source term that takes into account the contribution of the interplanetary shock as a particle accelerator.

The interplanetary transport of energetic particles has also been modeled using the Monte Carlo technique. Torsti et al. (1996) used the Monte Carlo method to simulate the focused transport of energetic particles. The development of this technique was followed by models from Kocharov et al. (1998) and Vainio (1998). More recently, similar approaches have been adopted by Maia et al. (2007) and Agueda et al. (2008).

[3]Several more assumptions were needed to obtain these results; among them: the parallel mean free path of the particles should be much smaller than the heliocentric distance of the observer; and the time of maximum intensity of the solution (Equation 3.13) should be much smaller than the adiabatic cooling time. See more details in Vainio et al. (2007).

[4]Hereafter, the focused transport equation, including adiabatic deceleration and solar wind convection effects, will be refered to as the 'focused transport equation'.

The Monte Carlo method is based on a kinematic approach: the simulation follows individual test particles as they move under the influence of a pre-described magnetic field. Using the guiding center approximation, for each simulated particle the code keeps track of spatial coordinate, time, pitch-angle and particle speed; no information about the phase angle around the magnetic field is tracked because gyrotropy is assumed.

The simulation begins by tracking the particles at the release site and at the time of injection. The particles are then moved during a Monte Carlo step (some models use a time step and some others use a spatial step) between scatterings off the magnetic irregularities occurring at a rate determined by the particle mean free path. Finally, particles are counted as they pass the 'observation site', which is frequently at Earth's distance from the Sun, but can of course be freely selected.

The different processes relevant to the transport of energetic particles along the IMF attain their simplest representation in different frames of reference. For example, the adiabatic guiding center motion in the average IMF has the simplest description in the frame corotating with the Sun, where the particle energy and the first adiabatic invariant are conserved. On the other hand, scattering off the irregularities of the magnetic field conserves particle energy in the frame moving with the scattering centers.

The Monte Carlo method is a powerful tool in dealing with complicated transport problems because it naturally allows the use of different reference frames. Specifically, the Monte Carlo method provides four principal advantatges with respect to the finite-differences method: (1) it is easy to implement, (2) it allows for individual control of all the transport processes, (3) it provides information on individual particle trajectories, and (4) it does not have the complication of numerical diffusion.

Nevertheless, the main disadvantage of the Monte Carlo method is that it is computationally very time consuming compared to the finite-differences method due to the repetition of algorithms and the large number of calculations involved. However, parallel programing and massive supercomputers can significantly speed up the calculations.

We have developed a Monte Carlo code to model solar near-relativistic electron events under different solar injection and interplanetary propagation conditions up to 1 AU. In the following sections, we describe the main features of this code.

3.2 Tracking particles

We consider an impulsive and isotropic injection of energetic particles at the radial distance of 2 $R_\odot$ from the center of the Sun. We assume that the source spectrum is a power law in

energy, $dN/dE \propto E^{-\gamma_s}$, with spectral index γ_s in the energy range $E_{\min} \leq E \leq E_{\max}$. After injection, NR electrons propagate along the IMF line. The code keeps track of the particles in the frame corotating with the Sun, where the particle speed is conserved during propagation. We move the particles in small radial Monte Carlo steps, δr (see section 3.4). After each step, we calculate the new particle position, $r = r_0 + \delta r$, the new pitch-angle cosine due to focusing $\mu(r; r_0, \mu_0)$, and the time elapsed during the propagation, $\delta t(r, \mu; r_0, \mu_0)$; all these quantities can be analytically calculated for a Parker spiral magnetic field (see Appendix A).

After computing the new position, pitch-angle cosine and time, we change the pitch-angle cosine of the particle due to scattering. The scattering is performed in the local solar wind frame, where the magnetic fluctuations are assumed to be static and, therefore, the particle speed is conserved. Before and after the scattering, particle velocity and pitch-angle cosine are transformed to the local solar wind frame and to the corotating frame, respectively. Expressions for the transformation of (μ, v) between the corotating frame and the local solar wind frame (represented by primes) are given by

$$\begin{cases} \gamma' = \gamma_u(\gamma - u_c \frac{\mu\gamma v}{c^2}) \\ v' = c\sqrt{1 - 1/\gamma'^2} \\ \mu' = \frac{\gamma_u \gamma}{\gamma'} \frac{1}{v'}(\mu v - u_c) \end{cases} \tag{3.14}$$

where c is the speed of light, $\gamma = 1/\sqrt{1 - v^2/c^2}$, $\gamma' = 1/\sqrt{1 - v'^2/c^2}$, $\gamma_u = 1/\sqrt{1 - u_c^2/c^2}$ and u_c is the relative velocity between the corotating frame and the local solar wind frame, given by

$$\vec{u_c} = u\hat{r} - \Omega r\hat{\phi} = u_c\hat{z} \tag{3.15}$$

where Ω is the angular velocity of solar rotation, $\hat{z}$ is the unitary vector along the outward tangent to the local magnetic field, and $\hat{r}$ is the unitary vector along radial direction. Thus, $\vec{u_c}$ is parallel to the magnetic field at each point and

$$u_c = u \ \sec\psi(z) \tag{3.16}$$

where $\sec\psi(z)$ is defined in Equation (3.3). This change of frames of reference leads to a systematic decrease of the energy of the particle in the solar-wind reference frame as the particle moves away from the Sun (Ruffolo 1995).

The propagation of each particle along a spiral magnetic field line connecting to the observer is followed until the maximum simulation time is reached. We record the time, energy and pitch-angle cosine of the particle each time it reaches the 'observation site'.

3.3 Modeling pitch-angle scattering

3.3.1 Isotropic scattering

Under isotropic scattering, i.e. ν constant ($\nu = \nu_0$), the pitch-angle diffusion coefficient, $D_{\mu\mu}$, given by Equation (3.7), has a functional form of a downward-opening parabola and the parallel mean free path is given by $\lambda_\parallel = v/\nu_0$. A simple and efficient method to model isotropic pitch-angle diffusion in a Monte Carlo simulation is to consider an ensemble of particles, initially located at a given point in phase space. After a time step $\delta t \ll \nu^{-1}$, the distribution of particles around the "scattering axis" (the instantaneous propagation direction of the unscattered trajectory) is given by

$$F(\vartheta, \phi, \delta t)\, d\Omega = \frac{1}{2\pi\nu\delta t} \exp\left(-\frac{\vartheta^2}{2\nu\delta t}\right) \vartheta\, d\vartheta\, d\phi \tag{3.17}$$

where $\vartheta \in [0, \pi)$ is the angle between the scattering axis and the direction of propagation of the scattered particle and $\phi \in [0, 2\pi)$ is the phase-angle around the scattering axis (Torsti et al. 1996; Kocharov et al. 1998). Thus, to model the pitch-angle diffusion, we pick the values of ϑ^2 and ϕ in each scattering process from exponential and uniform distributions, respectively. If the particle originally has a pitch-angle cosine μ (measured in the local solar-wind frame), the new pitch-angle cosine, μ', is given by (Ellison et al. 1990)

$$\mu' = \mu \cos\vartheta + \sqrt{1-\mu^2} \sin\vartheta \cos\phi \tag{3.18}$$

The geometric details of the scattering process can be found in Vainio (1998).

3.3.2 μ-dependent scattering

In the case of μ-dependent scattering, the method is not as simple and efficient as in the isotropic case, because the derivatives of ν lead to additional changes in μ for each scattering process. A general method for this case is described in Kocharov et al. (1998) and in Vainio (1998), but it requires much smaller time steps than for the isotropic case (hence the computing load increases dramatically). Many models predict μ-dependent scattering frequencies with a minimum at $\mu = 0$ (e.g. Bieber et al. 1994; Ng & Reames 1995), including the standard QLT (Jokipii 1966). Thus, it is important to include the effects of a μ-dependent ν in the scattering model.

We have identified (Agueda et al. 2008) a special dependence of $\nu(\mu)$ that allows an efficient use of the isotropic scattering method while still capturing the essential features of reduced

scattering at $\mu = 0$. Taking

$$\nu(\mu) = \nu_0 \frac{|\mu|}{1 + |\mu|} \tag{3.19}$$

with ν_0 constant; then $D_{\mu\mu} = \nu_0|\mu|(1 - |\mu|)/2$, which consists of two downward-opening parabolae, in the range of $\mu \in [-1, 0]$ and $\mu \in [0, 1]$, respectively. The linear dependence of ν on μ when $\mu \simeq 0$ guarantees that particles are not able to cross $\mu = 0$ by scattering, and that they remain in their initial hemisphere during each scattering process. A coordinate transformation

$$\eta = \begin{cases} 2\,(\mu - \frac{1}{2}), & \mu \geq 0 \\ \\ 2\,(\mu + \frac{1}{2}), & \mu < 0 \end{cases}$$

gives $-1 \leq \eta \leq 1$ and

$$D_{\eta\eta} = \left(\frac{d\eta}{d\mu}\right)^2 D_{\mu\mu} = \frac{1}{2}\nu_0(1 - \eta^2). \tag{3.20}$$

This transformation allows the use of the isotropic scattering method with a scattering frequency ν_0, but μ being replaced by η, in both hemispheres.

Adding another isotropic scattering process over the full range of μ with $\nu = \epsilon\nu_0$ yields the total scattering frequency

$$\nu(\mu) = \nu_0 \left(\frac{|\mu|}{1 + |\mu|} + \epsilon\right). \tag{3.21}$$

This means that we use Equations (3.17) and (3.18) twice, once for the η-process (with scattering rate ν_0) over one hemisphere and once for the μ process (with scattering rate $\epsilon\nu_0$) over the whole sphere. The three different components of the scattering rate (the two hemispheric processes and the one acting over the whole sphere) can be interpreted as due to different wave modes in the system and therefore, represent different scattering processes. Thus, to the lowest order in δt, operator splitting can be applied and each scattering process can be handled separately.

The functional dependence of $\nu(\mu)$ allows us to model a range of scattering conditions, from quasi-isotropic ($\epsilon \geq 0$) to fully anisotropic ($\epsilon = 0$, totally decoupled hemispheres). In this approach, the parallel mean free path can be expressed in terms of ν_0 and ϵ, as

$$\lambda_{\parallel} = \frac{3v}{4} \int_{-1}^{+1} \frac{1-\mu^2}{\nu(\mu)}\, d\mu = \frac{v}{\nu_0}\, \phi(\epsilon) \tag{3.22}$$

where $\phi(\epsilon)$ has the analytical form

$$\phi(\epsilon) = \frac{3}{2} \int_0^1 \frac{1-\mu^2}{\frac{\mu}{1+\mu} + \epsilon} d\mu = \frac{1}{4(1+\epsilon)^4} \left[4\epsilon^3 + 15\epsilon^2 + 12\epsilon + 1 + 6(1+2\epsilon) \ln\left(\frac{1+2\epsilon}{\epsilon}\right) \right]$$

Figure 3.3(a) displays the isotropic pitch-angle diffusion coefficient versus the pitch-angle cosine for $\lambda_{\parallel} = 0.5$ AU, together with the diffusion coefficient of two μ-dependent scattering models defined by $\epsilon = 0.10$ and $\epsilon = 0.01$. From this figure, it can be seen that in these two latter cases, $D_{\mu\mu}$ reaches its maximum value around $\mu \sim \pm 0.5$ and that $D_{\mu\mu}(\mu = 0) \neq 0$. Note that when $\mu \sim 0$, $D_{\mu\mu}$ has larger values for $\epsilon = 0.10$ than for $\epsilon = 0.01$.

PADs can be utilized to study the effect of different shapes of the pitch-angle diffusion coefficient on the transport of energetic particles. In the steady-state, Equation (3.4) can be analytically solved for the spatially integrated pitch-angle distribution, $F(\mu) = dN/d\mu$, under the assumption of constant focusing length[5]. In this case, the Fokker-Planck equation is given by

$$\frac{\partial}{\partial \mu} \left(\frac{1-\mu^2}{2L} v F \right) = \frac{1}{2} \frac{\partial}{\partial \mu} \left((1-\mu^2) \nu \frac{\partial F}{\partial \mu} \right). \tag{3.23}$$

The integration of this equation yields

$$F(\mu) = F_0 \exp\left(\frac{v}{L} \int_0^{\mu} \frac{d\mu'}{\nu} \right) \tag{3.24}$$

In the case of isotropic scattering ($\nu = v/\lambda_{\parallel}$)

$$F(\mu) = F_0 \exp\left(\frac{\lambda_{\parallel}}{L} \mu \right) \tag{3.25}$$

whereas in the case of μ-dependent scattering $F(\mu) = F_0\, e^{G(\mu)}$, where

$$G(\mu) = \text{sign}(\mu)\, \frac{\lambda_{\parallel}}{L\, \phi(\epsilon)}\, \frac{1}{1+\epsilon} \left[|\mu| + \frac{1}{1+\epsilon} \ln\left(1 + \frac{|\mu|(1+\epsilon)}{\epsilon} \right) \right] \tag{3.26}$$

[5]The focusing length is constant if the strength of the magnetic field decays exponentially along the distance measured along the field line (see Equation 3.5).

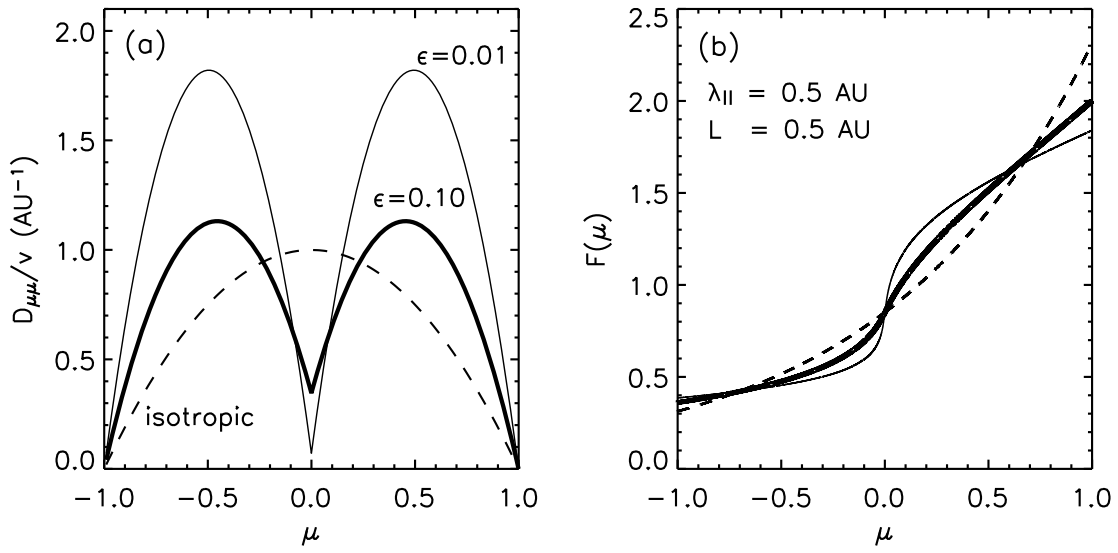

Figure 3.3: (a) $D_{\mu\mu}$ versus μ for $\lambda_{\parallel}$ = 0.5 AU; isotropic (dashed line) and μ-dependent scattering cases with ϵ = 0.10 (thick line) and ϵ = 0.01 (thin line); (b) Steady-state PADs derived for the same scattering cases depicted on the left. The focusing length is assumed to be L = 0.5 AU.

The relation between the scattering coefficient and the steady-state PADs is illustrated in Figure 3.3(b), which shows the normalized steady-state PADs for the pitch-angle diffusion coefficients displayed in Figure 3.3(a). In this case, we assume that L = 0.5 AU and $\lambda_{\parallel}$ = 0.5 AU. As it can be seen, the PADs approach an S-shape as the values of ϵ become smaller.

Figure 3.4 shows the normalized PADs in the case of isotropic scattering (dashed line) and μ-dependent scattering with ϵ = 0.01 (solid line) for different values of the parallel mean free path. The focusing length is assumed to be constant, L = 0.5 AU, and the parallel mean free path varies from 0.1 AU (left panel) to 0.7 AU (right panel). The higher the mean free path, the steeper the PADs due to the increasing relevance of the focusing effect.

3.3.3 Particle mean free path

We use the mean free path of the particles to parametrize the scattering frequency in the Monte Carlo model. For a given scattering model, the level of diffusion can be adjusted by changing the value of ν_0, which is derived from the value of the $\lambda_{\parallel}$. Following previous works (e.g. Palmer 1982; Beeck et al. 1987; Kallenrode et al. 1992) we take the radial mean free path, λ_r, to be constant in position. Therefore, the mean free path parallel to the IMF line, $\lambda_{\parallel} = \lambda_r \sec^2 \psi$, increases with radial distance. Thus, in our model $\lambda_{\parallel}$ varies with position and so does ν_0. We also assume that $\lambda_{\parallel}$ is independent of the energy, in accordance with the results derived by Dröge (2003) for NR electrons.

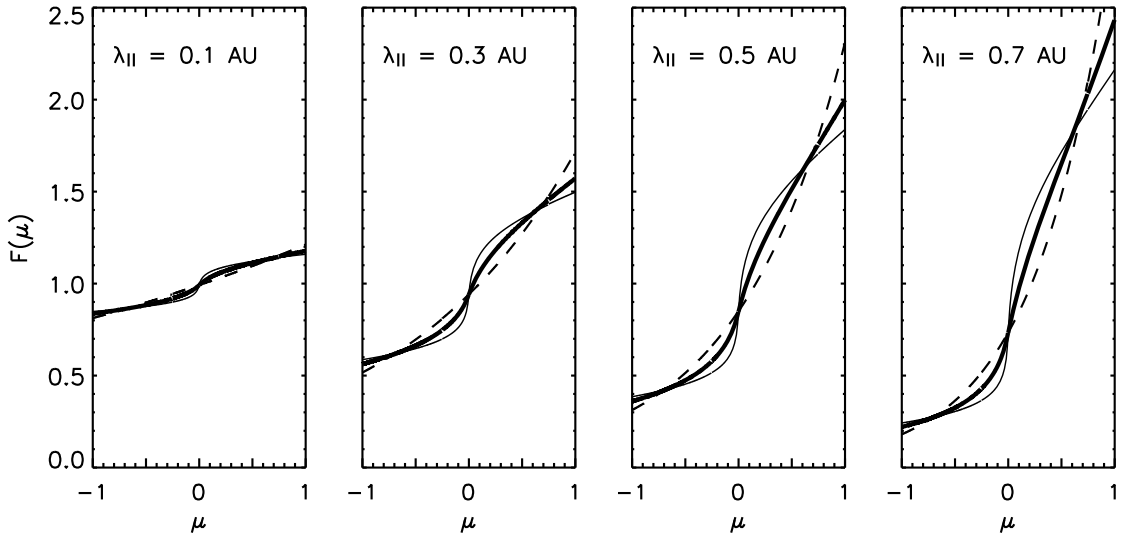

Figure 3.4: Normalized PADs in the case of isotropic scattering (dashed line), μ-dependent scattering cases with $\epsilon = 0.10$ (thick line) and $\epsilon = 0.01$ (thin line) for different scattering to focusing ratios. The parallel mean free path increases from left to right and $L = 0.5$ AU.

The focusing length of the Parker IMF is given by $L \simeq r/2$ inside 1 AU, whereas it is given by $L \simeq r^2/a$ beyond 1 AU (see Appendix A). The strong magnetic focusing effect close to the Sun ($L \ll \lambda_\parallel$) causes the initially injected distribution of energetic particles to become a beamlike anisotropic distribution shortly after its release. Thus, many SEP events show highly anisotropic distributions during their initial phase with the average pitch-angle cosine of the particles remaining close to $|\mu| = 1$ (outwards). The relationship between the pitch-angle diffusion coefficient $D_{\mu\mu}$ and the parallel mean free path $\lambda_\parallel$ given in Equation (3.9) is valid in the case of strong scattering and thus isotropic PADs. Under weak scattering conditions, the mean free path only gives a crude measure of the scattering strength. In this case, specific functions describing the pitch-angle diffusion coefficients should be given, in particular in the range close to $\mu \sim 1$.

It is possible to define a phenomenological scattering length to illustrate the strength of scattering near $|\mu| = 1$ as $\lambda_1(r) = v/\nu(1, r) \approx 2v/\nu_0$. Figure 3.5 plots the values of λ_1 as a function of the radial distance for two μ-dependent scattering models (with $\epsilon = 0.10$ and 0.01) together with the radial evolution of $\lambda_\parallel$ and L for $\lambda_r = 1.0$ AU. Note that for the isotropic model, $\lambda_1 = \lambda_\parallel$. For the two μ-dependent scattering models, the scattering length λ_1 gives an estimate of the beam isotropization length within a single hemisphere, whereas $\lambda_\parallel$ is more related to the scattering rate across $\mu = 0$.

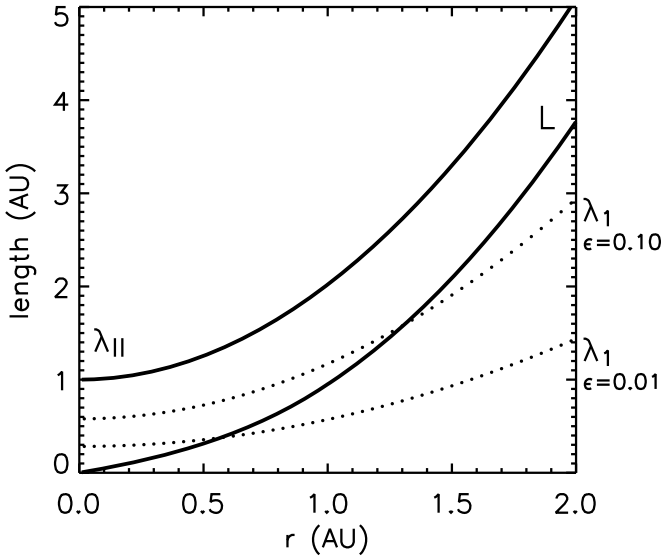

Figure 3.5: Focusing length, L, and parallel mean free path, $\lambda_\parallel$, for a constant radial mean free path $\lambda_r = 1.0$ AU. Dependence of the scattering length, λ_1, on the radial distance for two μ-dependent scattering models with $\epsilon = 0.10$ and $\epsilon = 0.01$ (dotted lines).

3.4 Monte Carlo radial step

The selection of the Monte Carlo radial step, δr, has to be handled carefully so that mirroring particles are given the chance to scatter before crossing $\mu = u_c/v$ (if $\mu = 0$ in the corotating frame, $\mu = -u_c/v$ in the local solar wind frame). This requirement is important in the case of μ-dependent scattering, where mirroring particles receive special treatment. Thus, the change in pitch-angle cosine, $\delta\mu$, is kept

$$\delta\mu \leq \frac{u_c}{v} \tag{3.27}$$

in one Monte Carlo step. Taking into account that $\dot{\mu} = (1 - \mu^2)v/2L$, Equation (3.27) can be written as

$$\frac{v\delta t}{4L} \leq \frac{u_c}{2v} \tag{3.28}$$

Then, as $\delta r = \delta z \cos\psi$ and $\dot{z} = \mu v$, considering Equation (3.28), the Monte Carlo radial step can be expressed as

$$\delta r \simeq 2L \frac{u_c}{v}\left(|\mu_0| + \frac{u_c}{2v}\right)\cos\psi \tag{3.29}$$

For a Parker spiral IMF, $L \simeq r/2$ close to the Sun (see Appendix A), then

$$\delta r \simeq r \, \frac{u_c}{v} \, \left(|\mu_0| + \frac{u_c}{2v} \right) \cos\psi \tag{3.30}$$

In a compromise between accuracy and computing time, we adopt

$$\delta r = \min\left(\frac{u_c}{v} \max(r_0, 0.3), 0.1\lambda_r \right) \cdot \left(|\mu_0| + \frac{u_c}{2v} \right) \cos\psi \tag{3.31}$$

Here δr is always positive and it holds for particles moving away from the Sun ($\mu_0 > 0$). When particles are moving toward the Sun ($\mu_0 < 0$), we take $-\delta r$ radial steps. If $\mu_0 < 0$ and the new position, $r_0 - \delta r$, is beyond the mirror point, r_m, we take $\delta r = r_m - r_0$.

3.5 Counting particles

The method of registration consists of counting particles when they are within the interval $r \in [r_\oplus - \Delta r/2, r_\oplus + \Delta r/2]$, around the point of observation $r_\oplus$. This means that we consider all particles contained in a volume $\sigma(r_\oplus)\Delta z$, where $\Delta z = \Delta r \, \sec\psi_\oplus$.

Particles are registered in a three dimensional array with dimensions (t, E, α), that is, time, energy and pitch-angle, respectively, when they are inside the registration volume. The bin sizes Δt, ΔE and $\Delta\alpha$ of the registration matrix can be chosen according to the problem we intend to study. We choose to bin the pitch-angle cosine in 20 bins ($\Delta\alpha = 9°$) in order to get PADs with high μ-resolution when $\mu \to \pm 1$. This is necessary in order to achieve an accurate modeling of the angular distributions in the case of large mean free paths. The time resolution is taken to be 72 s and the energy bins are chosen to match the electron channels of the LEFS60 telescope. The code allows the selection of different Δt, ΔE and $\Delta\alpha$ bin sizes to allow the study of other scenarios.

We express the results of the simulation in terms of near-Earth differential intensities but the same expressions can be used for the calculation of differential intensities observed at different radial positions of the observer. The differential intensity, δI, observed at position z and at a given time t (i.e. the number of particles per unit momentum, unit solid angle, and unit volume) is defined by

$$\delta I(z, t) = \frac{dN}{dp \, d\Omega \, d^3x} \tag{3.32}$$

Replacing $dE = v \, dp$ and $d\Omega = 2\pi \, d\mu$, this equation can be expressed in terms of the energy and the pitch-angle cosine as

$$\delta I(z,t) = \frac{v}{2\pi}\,\frac{dN}{dE\;d\mu\;d^3x} \tag{3.33}$$

As $d^3x = \sigma(r)\,dz$, integrating over time, we obtain the differential intensity measured around the position of the observer in a time interval, Δt,

$$\frac{1}{\Delta t}\int_t^{t+\delta t} \delta I\,dt \simeq \sum_{z\in[z-\Delta z, z+\Delta z]} \frac{v\delta t}{2\pi\sigma\Delta t}\,\frac{N}{dE\;d\mu\;dz}$$

Thus, each particle must be weighted by the factor $v\delta t$ when registered. The cross-sectional area of the flux tube at a given position is given by $\sigma(r) = r^2\cos\psi$ for a 1 sr solid angle cross sectional area at the solar surface.

Hence, the near-Earth differential intensity, i.e. the number of particles per unit time, unit energy, unit solid angle, and unit area, is given by

$$I = \frac{1}{r_\oplus^2}\frac{\hat{N}_{v\;\delta t}/\Delta r}{\Delta t\;\Delta E\;2\pi\Delta\mu}$$

where $\hat{N}_{v\;\delta t}$ is the $E-\mu-t$ matrix of the registered particles per total number of simulated particles; the subscript $v\;\delta t$ indicates that each particle has been weighted by $v\;\delta t$ when registered in the matrix; Δt, ΔE and $\Delta\mu$ correspond to the bin sizes of the registration matrix.

We give the result per total number of simulated particles, in order to get the result of the simulation in terms of the Green's functions for particle transport normalized to one particle injected per steradian at the solar surface.

This method requires that $\delta r \ll \Delta r$, in order to count each particle passing the spacecraft's position at least once; since δr is always below 0.003 AU (Equation 3.31), we adopt $\Delta r = 0.025$ AU.

3.6 Scheme of the code and simulation parameters

The general structure of the Monte Carlo particle transport code is summarized as follows:

1. Pick a set of source variables (initial state of a new particle): $(m,q) \leftarrow (m_0,q_0)$, $r \leftarrow r_0$, $\mu \leftarrow \mu_0$, $E \leftarrow E_0$ and $t \leftarrow 0$
2. Follow the particle along the IMF line during a Monte Carlo radial step δr: $r \leftarrow r + \delta r$
3. Calculate the advance in time δt: $t \leftarrow t + \delta t$

4. Calculate the new pitch-angle cosine resulting from focusing.

5. Perform scattering.

6. Update the matrix of observations, when necessary.

7. Start over from (2) until the maximum simulation time is reached.

8. Start over from (1) until the total number of injected particles is reached.

This procedure is general, thus, the code is suitable for the study of different types of SEP, although in this work it is applied to solar NR electrons. The input parameters necessary to simulate the initial state of a particle are: the type of particle (mass, m_0, and charge, q_0), the radial position of the source (r_0), the pitch-angle distribution of the source population and the energy spectrum ($dN/dE \propto E^{-\gamma_s}$, characterized by the spectral index γ_s).

For a given particle event it is possible to estimate an upper limit of the spectral index of the source, γ_s, from the calculation of the differential intensity spectrum of the observational differential intensities. The differential intensity spectral index is computed by fitting a power-law to the maximum spin-averaged intensity observed by the telescope in each energy channel, for example. If we assume that the mean free path is independent of the energy and that the effects of adiabatic deceleration on NR electrons are negligible, then the energy spectrum of the particles is not modified by their transport along the IMF and the two spectral indices are equal[6].

The code needs several other input parameters to fix the characteristics of the particle transport: solar wind speed (u), pitch-angle scattering model and mean free path (λ_r or $\lambda_\parallel$) as a function of distance and energy; steps 2 through 5 are controlled by these parameters.

Finally, the radial position of the observer and the registration bins (in time, energy and pitch-angle), as well as the maximum simulation time must also be provided as input parameters.

The simulation code is written in Fortran90 (to take advantage of its object oriented capability) and it has been run on a HP CP4000 machine under the PGF90 compiler in the Centre de Supercomputació de Catalunya[7].

[6]For further applications (see for example Chapter 5), we would like to note that since the differential intensity spectral index is defined in terms of momentum ($dN/dp \propto E^{-\gamma}$) instead of the energy, then $\gamma_s = \gamma + \frac{1}{2}$ since for non relativistic particles ($E \ll mc^2$)

$$\frac{dN}{dp} = \sqrt{\frac{2E}{m}}\,\frac{dN}{dE}.$$

[7]`http://www.cesca.es/`

3.7 Code testing

3.7.1 Analytical solutions

The particle transport code has been verified by checking that it reproduces the analytical steady-state solution of the Fokker-Planck equation for the spatially integrated pitch-angle distribution. The comparison of the analytical distributions (given by Equation 3.24) with the distributions obtained by the Monte Carlo simulations for the three scattering models show good agreement. As an example, Figure 3.6 shows the isotropic scattering case (left panel) and the μ-dependent scattering case with $\epsilon = 0.10$ (right panel). The code was run with $L = \lambda_{\parallel} = 0.5$ AU and simulation running time $t = 100L/v$, long enough to reach the steady-state.

We also verified that the simulation code reproduces the scaling law of the time-integrated flux with the distance obtained from the focused transport equation. If we assume steady-state conditions and Equation (3.4) is integrated over time and over μ, we obtain

$$\frac{\partial}{\partial z}\int_{-1}^{+1} \mu v F d\mu + \int_{-1}^{+1} \frac{1-\mu^2}{2L} v \frac{\partial F}{\partial \mu} d\mu = 0 \tag{3.34}$$

where $F = \int_0^{\infty} f\, dt$. Final integration gives

$$\left(\frac{\partial}{\partial z} + \frac{1}{L}\right)\mathcal{F} = 0 \tag{3.35}$$

where $\mathcal{F} = \int_{-1}^{+1} \mu v F d\mu$ is the time-integrated net flux. Taking into account that $\sigma(r) \cdot B(r)$ is constant, then

$$\frac{1}{L} = -\frac{1}{B}\frac{\partial B}{\partial z} = \frac{1}{\sigma}\frac{\partial \sigma}{\partial z} \tag{3.36}$$

and therefore

$$\frac{\partial}{\partial z}(\sigma\mathcal{F}) = 0 \quad \Longrightarrow \quad \sigma\mathcal{F} = \text{constant}$$

This means that the time-integrated net flux scales like $\mathcal{F} \propto \sigma^{-1} \propto B$.

This scaling law can be directly compared with the results of the Monte Carlo simulation. For this purpose, we assume that electron injection at the root of an interplanetary flux tube can be parametrized using the Reid–Axford profile (Reid 1964)

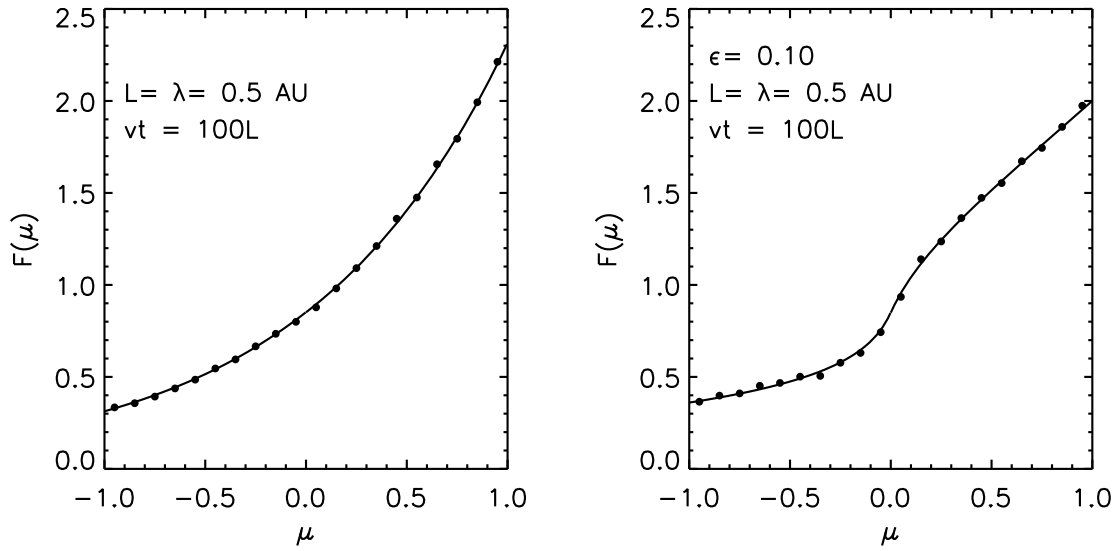

Figure 3.6: Simulated (dotted) and analytical (line) normalized steady-state pitch-angle distributions for a system with constant focusing length and isotropic scattering (left) or μ-dependent scattering with $\epsilon = 0.10$ (right).

$$q(t) = \frac{N}{t} \exp\left(-\frac{\beta}{t} - \frac{t}{\tau}\right) \tag{3.37}$$

where β and τ parameters represent the rise and decay time scales respectively, and N is a normalization constant; we adopt $\beta = 4.2$ min and $\tau = 1.2$ min. We also assume a constant radial mean free path, $\lambda_r = 0.6$ AU, independent of energy. With this set of parameters (see more details in Vainio et al. 2007), we record the differential intensities observed at different radial distances: 0.2, 0.3, 0.7 and 1.0 AU. Then, we determine the time-integrated net-flux at these radial distances. Figure 3.7 shows the results obtained in the four E' energy channels of the LEFS60 telescope; as can be seen, the time-integrated net flux in the simulation follows the behavior that the focused transport theory predicts and scales like $\propto \sigma^{-1}$.

Finally, we also verified the particle transport code by checking that it reproduces the analytical solution that describes the effect of adiabatic deceleration when particles' PADs are nearly isotropic. If particles have an isotropic PAD in the solar wind frame, the average rate of adiabatic deceleration is given by

$$\langle \dot{p} \rangle = -\frac{p}{3} \nabla \vec{u} \tag{3.38}$$

where $\vec{u}$ is the solar wind velocity and p is the particle momentum in the solar wind frame (Parker 1965; Dorman 1965). If we assume the speed of the wind, $|\vec{u}| = u$, to be constant and its direction to be field aligned, we can write

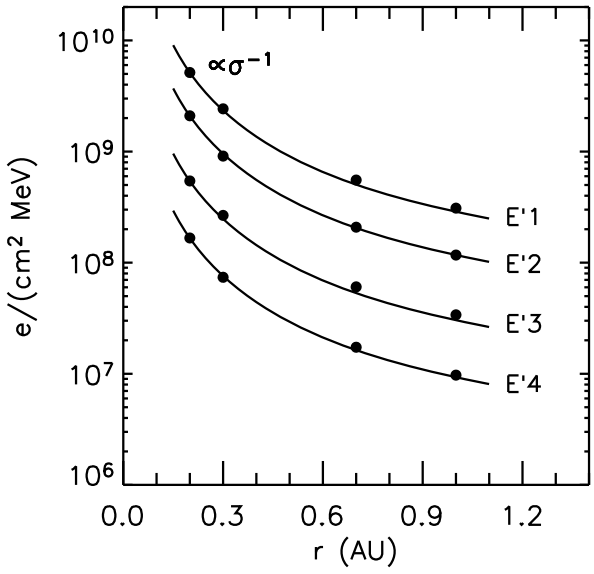

Figure 3.7: Time-integrated net flux as a function of radial distance in several energy channels (dots). Solid line shows $\propto \sigma^{-1}$ behavior.

$$\nabla \vec{u} = \frac{1}{\sigma(z)} \frac{\partial}{\partial z} (\sigma(z) \cdot u) = \frac{\partial u}{\partial z} + \frac{1}{\sigma(z)} \frac{\partial \sigma}{\partial z} u = \frac{u}{L} \tag{3.39}$$

where σ is the cross-section area of the magnetic flux tube and L is the focusing length. Then, taking L to be constant and much longer than the parallel mean free path, the expected rate of deceleration is

$$\langle \dot{p} \rangle = -\frac{p}{3L} u \tag{3.40}$$

giving, for $p(t = 0) = p_0$,

$$\langle p \rangle (t) = p_0 \cdot \exp\left(-\frac{u}{3L} t\right) \tag{3.41}$$

To check this analytical solution, we assume that particles are injected at $t = 0$ with fixed momentum, p_0, and isotropic PAD in the solar wind frame. The wind speed, u, is constant along the field and the focusing length, L, is also constant; we assume $u = 400$ km s^{-1} and $L = 1$ AU. We assume a constant parallel mean free path much smaller than the focusing length, $\lambda_{\parallel} = 0.1$ AU.

Based on the assumptions listed above, we compute the mean momentum of particles in the system as a function of time and check that it decays exponentially according to Equation (3.41); equivalently, we can compute the mean kinetic energy as a function of time, where

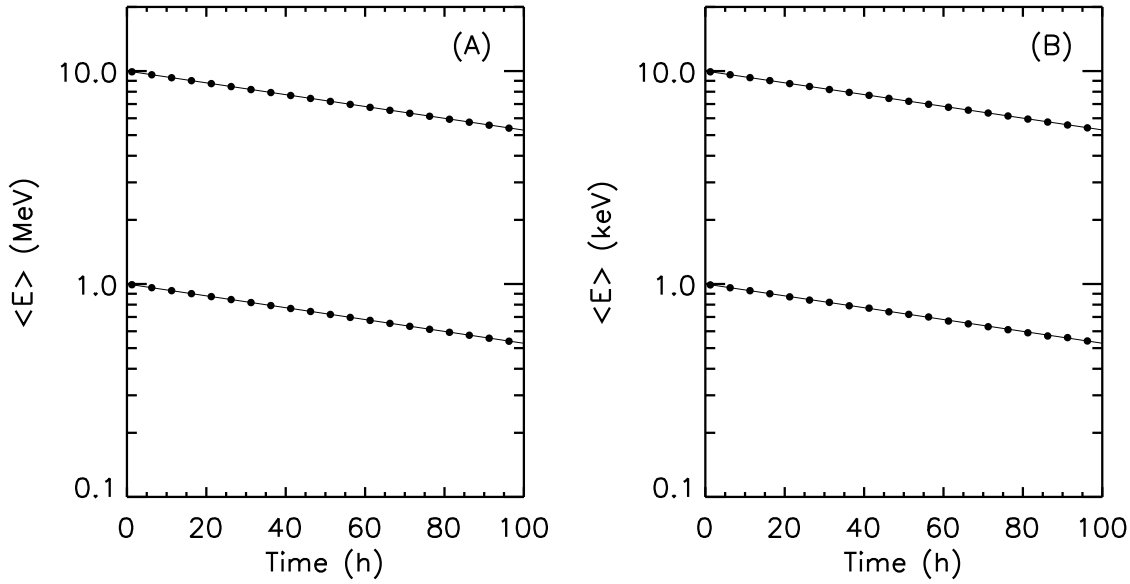

Figure 3.8: Average energy, <E>, of particles in the solar wind frame versus time (solid line) for an isotropic mono-energetic injection of (A) protons at $E_0 = 10$ MeV and $E_0 = 1$ MeV, and (B) electrons at $E_0 = 10$ keV and $E_0 = 1$ keV. Dots show the results of the model.

$$E = \sqrt{p^2c^2 + m^2c^4} - mc^2.$$

Figure 3.8 shows the average energy of the particles in the solar wind frame, <E>, versus time for isotropic mono-energetic injection of protons with initial kinetic energy $E_0 = 10$ MeV and $E_0 = 1$ MeV (panel A) and electrons with initial kinetic energy $E_0 = 10$ keV and $E_0 = 1$ keV (panel B). Solid lines show the analytical solution, whereas dots show the results of the model. We find good agreement between theory and simulation.

3.7.2 Comparison with a finite-differences transport code

The Monte Carlo transport code was also tested against a finite-difference numerical method to solve the focused transport equation deduced by Ruffolo (1995). The variables selected for comparison were the spectral indices that describe the radial dependences of peak intensities and fluences of solar energetic particle events observed inside 1.6 AU. In particular, we verified the radial dependences obtained by Lario et al. (2007).

The main assumptions made by Lario et al. (2007) are: (1) the particle injection takes place at the root of an Archimedean spiral magnetic field (defined by $u = 431$ km s^{-1}); (2) the injection of particles follows a Reid-Axford profile defined by the rise (β) and decay (τ) time scales; (3) the energy spectrum at the source is $dN/dp \propto p^{-4.8}$, where p is the particle momentum; (4) the pitch-angle scattering is described by means of the diffusion coefficient given by Equations (3.7) and (3.8) with $q = 1.5$; and (5) the mean free path $\lambda_{\parallel}$ is considered

to be constant along the flux tube and independent of the energy.

Lario et al. (2007) considered protons injected with energies ranging from 4 to 48 MeV and solved the focused transport equation for two energies: 8.3 MeV and 34.6 MeV. Lario et al. (2007) set several observers at radial distances r = 0.3, 0.4, 0.5, 0.6, 0.7, 0.8, 1.0, 1.2, 1.4, and 1.6 AU along the flux tube where energetic particles propagate. They considered four different cases:

- *Case 1*: β = 1.5 h, τ = 0.2 h, and $\lambda_{\parallel}$ = 0.1 AU;
- *Case 2*: β = 1.5 h, τ = 1.5 h, and $\lambda_{\parallel}$ = 0.1 AU;
- *Case 3*: β = 1.5 h, τ = 0.2 h, and $\lambda_{\parallel}$ = 1.0 AU;
- *Case 4*: β = 1.5 h, τ = 1.5 h, and $\lambda_{\parallel}$ = 1.0 AU.

Taking the same injection and transport parameters as in Lario et al. (2007), we simulate the same four cases. Particularly, we use the μ-dependent scattering model with ϵ = 0.05 to simulate the reduced scattering rate around μ = 0. Figure 3.9 shows shape of the standard pitch-angle diffusion coefficient used by Lario et al. (2007) versus the pitch-angle diffusion coefficient corresponding to a μ-dependent scattering model with ϵ = 0.05. The two coefficients are very similar. However, the standard diffusion coefficient used by Lario et al. (2007) predicts a smaller scattering rate of pitch-angle scattering around $\mu \sim 0$ than our model does. Due to this unavoidable difference, small differences could appear between the results provided by the two models.

We assume two energy ranges, 4.6–15.0 MeV and 25.0–48.0 MeV, for particle registration that comprise the two energies studied by Lario et al. (2007). Differences between the results provided by the two models may also arise because the Monte Carlo model solves the transport equation for an energy range, while the finite-difference numerical method solves the transport equation using a grid of discrete values for the particle energy.

Figure 3.10(a) shows the 4.6–15.0 MeV omnidirectional time-intensity profiles registered by different observers located at different radial distances assuming β = 1.5 h, τ = 1.5 h and $\lambda_{\parallel}$ = 0.1 AU (case 4). Injection is assumed to start at t = 0. Black circles indicate the maximum intensity of the plotted time-intensity profiles, whereas gray circles indicate the maximum intensity of the event at the distances not plotted in the figure. The Monte Carlo event fluence is calculated as the integral over time of the omni-directional intensities. Figure 3.10(b) shows the radial dependence of peak intensities (black dots) and event fluences (white dots). Following Lario et al. (2007), we fit two power-laws ($\propto r^{-\alpha}$) to both the peak intensities

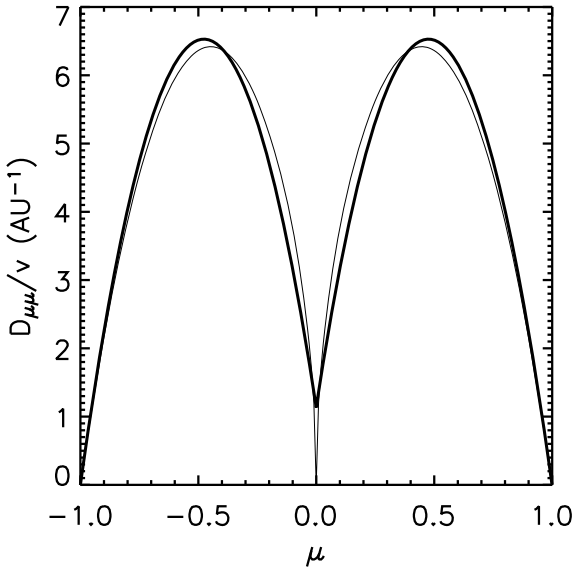

Figure 3.9: $D_{\mu\mu}$ versus μ for $\lambda_{\parallel}$ = 0.1 AU. Comparison of the $D_{\mu\mu}$ assumed by Lario et al. (2007) (thin line) with the $D_{\mu\mu}$ corresponding to a μ-dependent scattering model with ϵ = 0.05 (thick line).

and the fluences, the first one for the inner region (0.3 to 1.0 AU) and the second one for the outer region (1.0 to 1.6 AU).

Table 3.1 lists the power-law indices for each of the four cases. Columns identified by `'FD'` list the power-law indices obtained by Lario et al. (2007). The first column lists the spectral index of the inner region and the second column lists the spectral index of the outer region. Table 3.1 also lists the power-law indices obtained with the Monte Carlo transport code (column `'MC'`). Under similar assumptions, the two models provide very similar results. We remit to Lario et al. (2007) for a complete discussion about the effects of the different parameters on the values of the scaling indices.

Note, however, that for $\lambda_{\parallel}$ = 0.1 AU (Case 1 and 2), the peak intensities in the outer region do not obey the diffusion model, $\propto r^{-3}$; instead, they decrease with radial distance as $\propto r^{-3}$ to r^{-4}. This is in accordance with a previous observational study from Hamilton (1977). The more rapid radial decay is attributed to the solar wind effects (convection and adiabatic deceleration) that become more important the smaller the mean free path and the further the location of the observer from the Sun. For $\lambda_{\parallel}$ = 1.0 AU (Case 3 and 4), the power-law indices obtained by the two models are very similar.

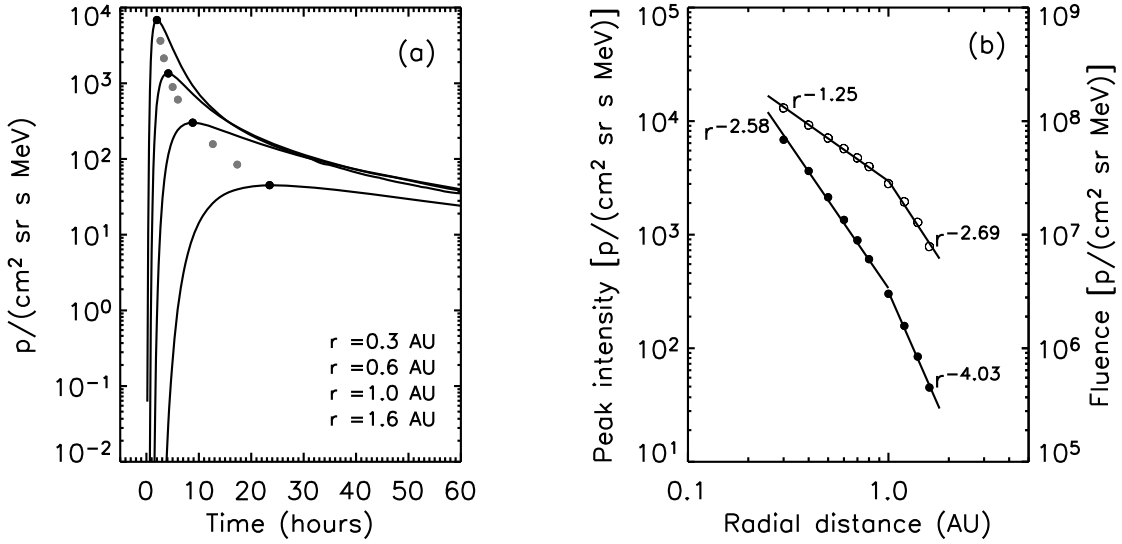

Figure 3.10: Monte Carlo model. Case 4: $\beta = 1.5$ h, $\tau = 1.5$ h and $\lambda_{\|} = 0.1$ AU. (a) Omnidirectional time-intensity profiles of the 4.6–15.0 MeV protons as observed at 0.3, 0.6, 1.0 and 1.6 AU. Black circles indicate the peak intensity observed at these radial distances, whereas gray circles indicate the maximum intensity at 0.4, 0.5, 0.7, 0.8, 1.2 and 1.4 AU. (b) Radial dependence of the peak intensities (black dots) and event fluences (white dots).

Table 3.1: Power-law index, α, for each case. FD (finite-differences) refers to the results obtained by Lario et al. (2007) and MC refers to the results obtained with our Monte Carlo transport code. For each energy, left/right column lists α in the inner/outer region (see text for details).

		FD	MC	FD	MC
Case		8.3 MeV	4.6–15.0 MeV	34.6 MeV	25.0–48.0 MeV
1	Peak	3.18 3.60	3.16 4.09	2.81 3.31	2.78 3.43
	Fluence	1.45 2.00	1.25 2.68	1.17 1.49	1.00 1.82
2	Peak	2.58 3.49	2.58 4.03	2.22 3.07	2.22 3.28
	Fluence	1.45 2.01	1.25 2.69	1.17 1.49	1.01 1.83
3	Peak	1.96 3.06	2.24 3.08	1.68 2.60	1.80 2.53
	Fluence	0.87 1.00	0.87 1.00	0.73 0.78	0.68 0.75
4	Peak	1.56 2.34	1.73 2.41	1.38 1.95	1.50 1.95
	Fluence	0.86 0.99	0.87 1.01	0.73 0.78	0.68 0.75